# Formation and Aging of Incipient Thin Film Wax-Oil Gels

**Probjot Singh, Ramachandran Venkatesan, and H. Scott Fogler**
Dept. of Chemical Engineering, University of Michigan, Ann Arbor, MI 48109

**Nagi Nagarajan**
Mobil Technology Company, Dallas, TX 75244

*A fundamental study of the deposition and aging of a thin incipient wax-oil gel that is formed during the flow of waxy oils in cooled pipes was performed. The solubility of high molecular weight paraffins in naphthenic, aromatic or paraffinic solvents is very low and decreases rapidly with decreasing temperature. This property of the paraffins leads to the formation of gels of complex morphology that deposit on the cold walls of the subsea pipelines during the flow of waxy crudes. This deposition reduces the pipe diameter and decreases the flow capacity of the pipe. These wax-oil gels contain a large fraction of oil trapped in a 3-D network structure of the wax crystals that behaves as a porous medium. After the incipient gel is formed, wax molecules continue to diffuse into this structure, thereby increasing its wax content. A model system of wax and oil mixture was used to understand the aging process of the wax-oil gels, which hardens the wax deposit with time. To understand the physics of the aging process for incipient thin-film deposits, a series of laboratory flow loop experiments was performed. The aging process was a counterdiffusion phenomenon with a critical carbon number above which wax molecules diffuse into the gel deposit and below which oil molecules diffuse out of the deposit. The aging rate of the gel deposit depends on the oil flow rate and the wall temperature. A mathematical model developed predicted the growth and wax content of the gel deposit on externally cooled pipe walls. The theory agreed with experiments excellently for thin gels.*

## Introduction

Solid deposition phenomena occur in many systems such as crystallization fouling of heat exchangers (Bott, 1997), frost formation (Lee et al., 1997) and scale deposition (El-Hattab, 1985). The deposition of crystals on heat exchanger surfaces is common in aqueous systems. When the cold surface of a heat exchanger is exposed to warm, moist air, a layer of frost deposits, resulting in a decrease in the efficiency of the heat exchanger. In petroleum production and processing, deposition of organic material (such as paraffin wax) in the flow lines reduces the flow efficiency. In this work, the fundamentals of the deposition of paraffin waxes during flow of waxy crude oils through cold pipelines are elucidated.

Thin film paraffin wax gels can be deposited from crude oil when the oil is exposed to cold temperatures. Crude oil is a complex mixture of hydrocarbons consisting of paraffins, aromatics, naphthenes, resins and asphaltenes. Among these groups of hydrocarbons, high molecular weight paraffins (waxes) are responsible for some of the problems that are encountered during transportation and processing of the crude oil. The high molecular weight paraffins have a low solubility in most of the aromatic, naphthenic, and other organic solvents at room temperatures. At off-shore reservoir temperatures (in the range of 70−150°C) and pressures (in the range of 8,000−15,000 psi, 55−103 MPa), the solubility of these compounds is sufficiently high to keep them fully dissolved in the mixture and the crude oil behaves as a Newtonian fluid with a low viscosity. Once the crude oil leaves the reservoir and flows through the tubing and subsea pipelines, its temperature begins to drop due to the cooler environment.

Correspondence concerning this article should be addressed to H. S. Fogler.

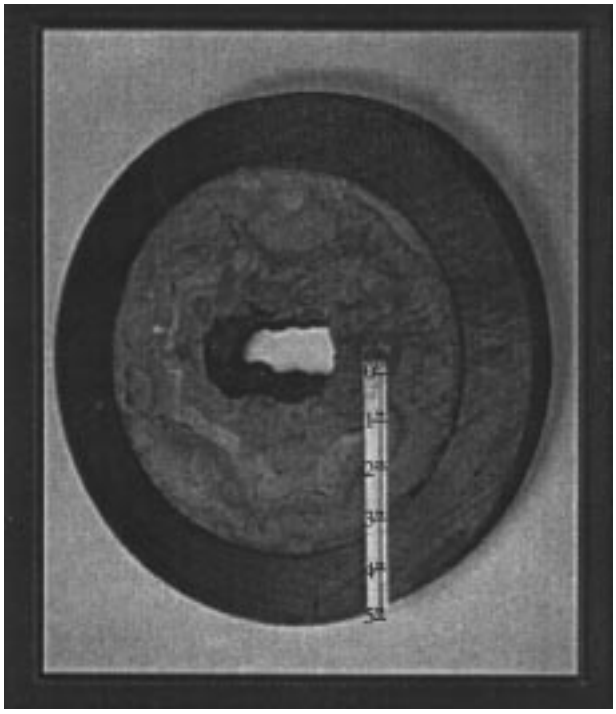

**Figure 1. Plugged pipeline.**

Inasmuch as the solubility of high molecular weight paraffins decreases drastically with decreasing temperatures, stable wax crystals are formed at low temperatures. The crystallization of paraffins leads to the formation of gels with a complex morphology. The gelation is due to the flocculation of orthorhombic wax crystallites that appear in the solution while cooling (Dirand et al., 1998). Observations with a cross-polarized microscope revealed that the crystallites have structures of platelets that overlap and interlock (Holder and Winkler, 1965a). Studies on distillate fuels show that as little as 2% of the precipitated wax is required to gel the fluid (Holder and Winkler, 1965b). A gel deposit with as little as 2% wax was also obtained from our laboratory flow experiments.

The formation of the paraffin gels, at the pipe-walls, plugs up the pipelines and restricts the flow. Figure 1 shows the wax buildup in a cutaway view of a pipeline segment retrieved from subsea. The magnitude of this problem can be gauged from the fact that the Lasmo Company (U.K.) had to abandon a platform at a cost of $100 million, due to recurring wax deposition problems in the pipelines. If mechanical techniques, such as pigging, are to be used to prevent wax buildup, an understanding of the rate of formation and the properties of the incipient gel is necessary.

A number of mechanisms have been proposed to elucidate wax deposition on pipe walls. These mechanisms include molecular diffusion, shear dispersion, Brownian diffusion, and gravity settling (Bern et al., 1980; Burger et al., 1981; Majeed et al., 1990). Wax particles start appearing in the crude oil when the bulk temperature drops below its cloud point (solubility limit). The deposition of the wax in the particulate state is determined by mechanisms such as shear dispersion, Brownian diffusion, and gravity settling. However, our experimental results confirm that particulate deposition is not significant for flow conditions encountered in oil pipelines on the ocean floor (also mentioned in Brown et al., 1993). Hence, gelation along with the molecular diffusion mechanism is currently our focus of attention.

A number of mathematical models have been developed that describe the deposition process. All of the models are based on the premise that wax-oil deposits have a constant wax content (Brown et al., 1993; Bern et al., 1980; Burger et al., 1981; Majeed et al., 1990; Svendsen, 1993; Ribeiro et al., 1997). The composition of the gel, as well the rate of gelation, depends on the conditions at which the gel is deposited. The wax-oil mixture gels with cooling, and the nature of this gel depends strongly on the cooling rate (Singh et al., 1999). The incipient wax-oil gel deposit contains a significant amount of oil trapped in a 3-D network structure of the wax crystals. Hence, the gel behaves as a porous medium in which wax molecules continue to diffuse due to the radial variation in temperature. Thus, the wax content of the deposited gel increases with time. This process is called aging of the gel deposit. In all existing models, the oil content of the deposit is used as an adjustable parameter to match results from flowloop experiments with model predictions. Inasmuch as these models assume a constant value for the oil content, they are not accurate and cannot be applied to predict the thickness profile and the nature and properties of the wax deposit (such as hardness, melting point, and heat of fusion), which can vary significantly with time. Selection of the technique to remove the deposits in the pipeline depends on the nature of the deposit and, hence, the prediction of properties of the wax deposits is essential. One such technique to remove the wax deposits has been described by Singh and Fogler (1998).

In order to understand the physics of wax deposition, a model wax-oil system was studied in the laboratory. This model wax-oil system was prepared by dissolving a sample of food grade wax (Mobil M140) into an oil solvent (a 3:1 mixture of mineral oil and kerosene). A laboratory flow loop was used to perform the wax deposition experiments. Wax deposits were analyzed for the critical carbon number using high-temperature gas chromatography (HTGC). It was found that a counterdiffusion phenomenon, in which wax molecules diffuse into the gel deposit and oil molecules diffuse out of the deposit, is responsible for aging. The aging rate of the gel deposit depends on the flow rate of the oil, as well as the wall temperature of the pipeline. Based on this physical model of the wax deposition, a mathematical model was developed to simulate the variation of the thickness and the wax content of the deposit with time. A system of coupled differential and algebraic equations of heat and mass transfer inside, as well as outside, the gel deposit has been developed. In this article, the flow loop experiments that were performed to understand the physics of the wax deposition process are described. The theory for the mathematical model is developed, and solution procedure is discussed. The theoretical model predictions are compared with the experimental results.

## Experimental Studies

### *Wax-oil mixture*

The wax-oil mixture is composed of heavy paraffin molecules and light oil molecules. The cloud point of the sys-

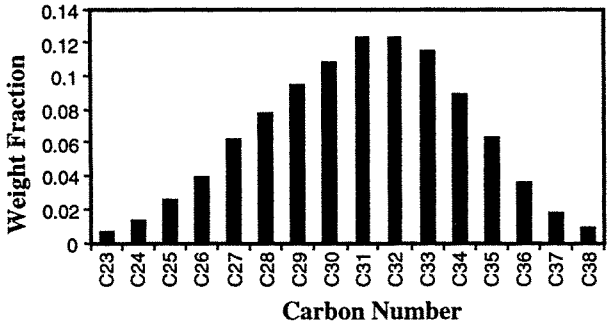


**Figure 2. Molecular weight distribution of the Food Grade Wax (Mobil M140).**

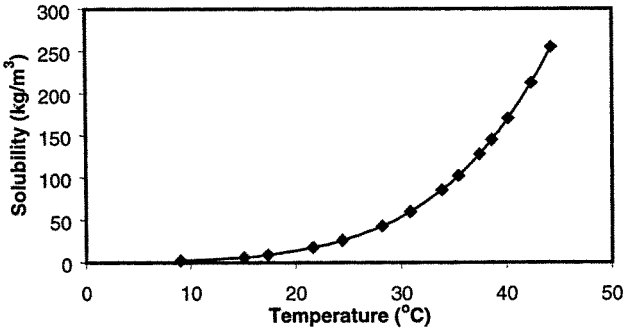


**Figure 4. Solubility of the food grade wax in the model oil solvent.**

tem has been defined as the temperature below which paraffin molecules start precipitating as wax crystals. The system is in a liquid phase above the cloud point, and a solid phase appears below this temperature. The wax-oil gel deposition occurs when the paraffins crystals deposit on the cold wall of the pipeline along with the oil trapped in the matrix of the crystals. In the laboratory flowloop, the bulk temperature of the wax-oil mixture is always higher than that of the cloud point. Hence, the fluid flow has been considered as a single liquid-phase flow. The wax-oil gel deposit has been considered as an immobile gel-phase material composed of wax crystals and trapped oils (Burger et al., 1981).

### *Materials*

*Food Grade Wax (Mobil M140).* The molecular weight distribution of this wax was obtained by a Varian 3800 high-temperature gas chromatograph and is shown in Figure 2. High-temperature high-resolution gas chromatography is commonly used to characterize paraffin deposits in petroleum production pipelines (Neto et al., 1994). Carbon number distribution of the wax had a range from 23 to 38 and weight average molecular weight was 435.

*Oil Solvent.* The oil solvent used for food grade wax was a 3:1 mixture of mineral oil (Blandol) and Kerosene. Density and viscosity of the oil mixture were 0.8385 g/cm$^3$ and 8.7 mPa·s, respectively, at room temperature. Figure 3 shows the high-temperature gas chromatograms of the wax and the oil used for our studies. The solubility of the food grade wax in this oil mixture obtained from batch experiments is shown in Figure 4. When the temperature of the wax-oil sample goes below the cloud point, wax starts precipitating out of the solution as wax crystal.

### *Laboratory flow loop*

The flow loop experiments simulate the gel deposition in the pipelines under cold environments. Figure 5 shows a sketch of the laboratory flow loop, which was used in the wax deposition study. A sample of the wax-oil mixture was first heated to 30–35°C in a stirred vessel. During a typical run, the stirred vessel was maintained at a temperature above the cloud point. A specified wax-oil mixture was pumped from the stirred vessel through the test section that was cooled by a heat exchange jacket. The mixture returned to the stirred vessel through a reference section. Both the test section and the reference section had 5/8 in. (16 mm) OD steel tubing, each 8 ft (2.4 m) long. Both sections had pressure taps connected to differential pressure transducers every 2 ft (2.4 m). The thickness of the gel deposit on the wall of the test section was determined from the increase in the differential pressure. A data acquisition system continuously recorded the wall temperature and inlet temperatures of the fluid along with differential pressure readings in the test and reference sections.

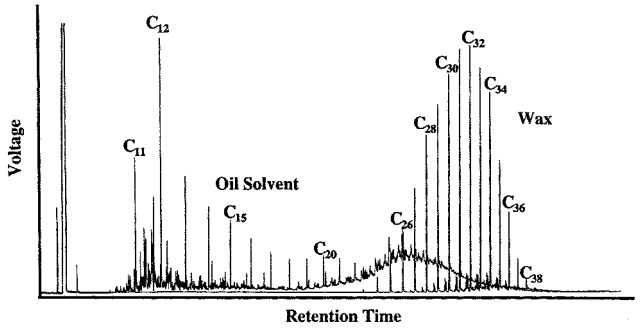


**Figure 3. Chromatograms from high-temperature gas chromatography.**

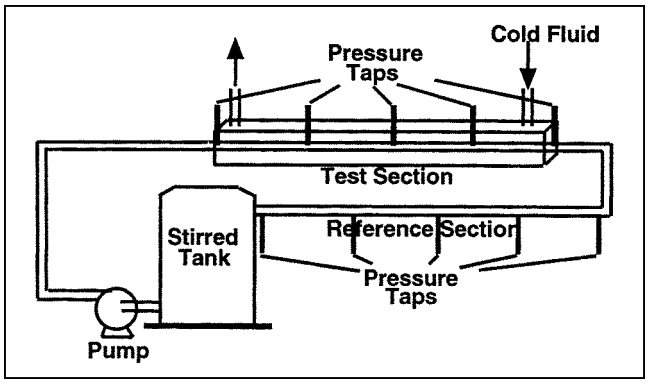


**Figure 5. Laboratory flow loop setup.**

## Physics of Wax Deposition

The solubility limit for a given condition, particularly temperature, is the cause for almost all examples of deposition previously discussed. The solubility of a solute is temperature-dependent and, in most cases, it increases with increasing temperature; hence, if a saturated solution of a salt is cooled, salt crystals separate out from the solution. When such a solid precipitate deposits on the surface, it traps a significant amount of solvent in the interstices of the crystals. The mechanism of the deposition process on a heat exchanger tube wall can be described by the following steps (Bott, 1997):

(1) Initial precipitation on the cold surface, resulting in a radial concentration gradient.
(2) Radial diffusion of salt towards the interface from the bulk.
(3) Internal diffusion inside the deposit through the trapped solvent.
(4) Desolvation of the salt in the deposit.
(5) Radial counterdiffusion of the trapped solvent away from the surface.

Steps 3 and 5 lead to hardening of the deposit, that is, increase of the solid content of the deposit.

The mechanism of frost deposition on a cold surface exposed to warm air can also be described by the above five steps. Frost deposition starts with the formation of ice columns of varying diameters and orientations. The air in contact with these sparsely distributed ice columns is stagnant and is analogous to the trapped solvent described above. These ice columns grow as more water vapor diffuses through the stagnant air and crystallizes, leading to an internal densification of the frost layer (Tao et al., 1993).

Wax deposition in cold flow lines is a similar deposition process. When a sample of waxy oil is cooled, it gels due to the formation of a network of wax crystals. Unlike in the case of the inorganic solutions, where there is hardly any interaction among salt crystals, the wax crystals have a strong interaction and affinity, resulting in the formation of the network. Although oil (solvent) and wax (solute) have a similar chemical nature, their molecular weights are quite different. Waxes have a higher molecular weight, and they tend to form stable wax crystals that interlock to form a solid network (Wardhaugh and Boger, 1991). The network of wax traps a large quantity of oil (Holder and Winkler, 1965). Hence, the initial stage of the deposition of the waxy oil mixture on a cold surface is the formation of a gel layer with a large fraction of trapped oil.

Waxy oil is a mixture of hydrocarbons of varying carbon numbers. When this mixture is cooled to a certain temperature, a fraction of hydrocarbons with carbon numbers above a certain value (the *critical carbon number*) precipitate out as stable crystals to form a gel with the remaining hydrocarbons trapped in the gel network. The formation of such gels on a cold surface is the first step of this deposition process. The trapped liquid acts as a medium for further diffusion of the heavier molecules into the gel. This diffusion of heavier molecules is accompanied by the counterdiffusion of the trapped oil out of the deposit. This process leads to an increase in the fraction of molecules with the carbon number greater than the critical carbon number, and a decrease in the fraction of molecules with the carbon number lower than the critical number in the gel. The critical carbon number would be different for different waxy oils, and is also a function of the operating conditions such as wall temperature. The diffusion process hardens the deposited gel with time, making the wax removal process difficult. The wax deposition process can be described by the following steps:

(1) Gelation of the waxy oil (formation of incipient gel layer) on the cold surface
(2) Diffusion of waxes (hydrocarbons with carbon numbers greater than the critical number) towards the gel layer from the bulk
(3) Internal diffusion of these molecules through the trapped oil
(4) Precipitation of these molecules in the deposit
(5) Counterdiffusion of de-waxed oil (hydrocarbons with carbon numbers lower than the critical number) out of the gel layer.

Again, the last three steps result in an increase of the solid wax content of the deposit.

Various mechanisms by which wax deposition could occur, such as molecular diffusion, shear dispersion, Brownian diffusion and gravity settling, have been proposed (Bern et al., 1980; Burger et al. 1981; Majeed et al., 1990). Mechanisms such as shear dispersion, Brownian diffusion, and gravity settling play a role only for particulate deposition of wax. However, our experimental results confirm that particulate deposition is not significant for flow conditions encountered in oil pipelines on the ocean floor. Hence, molecular diffusion is the predominant mechanism underlying the wax deposition process.

This section describes the physics of the incipient gel deposition and the various mechanisms by which aging of the gel deposit could occur, along with a detailed discussion of the experimental results. This discussion provides an excellent insight into the physics of the process and helps to identify the most dominant mechanisms involved in the aging of the wax deposit.

### *Formation of the incipient gel deposit*

When a warm wax-oil mixture comes in contact with a cold surface, a layer of the sample near the surface loses heat and temperature of the layer decreases rapidly, well below the cloud point of the mixture. This decrease in the temperature causes the layer to form a gel at the cold surface. This incipient gel is a complex network of wax crystals having a large volume fraction of oil trapped in it. The gel layer continues to grow until the pipe is partially plugged (c.f. Figure 1).

Formation of the incipient gel is only the first step in the deposition process. The gel was also found to harden with time (that is, aging). In order to determine whether or not the gel can be removed by mechanical means such as pigging, knowledge of the hardness of the gel is extremely important. Flow loop experiments were performed to observe the growth and aging of the gel deposit. A wax-oil mixture with 0.67 wt. % of wax entered the test section at a temperature of 22.2°C, where the wall temperature of the tubing was maintained at 7.2°C. Experiments for six different aging times of 2 h, 12 h, 1 day, 2 days, 3 days, and 5 days were carried out at a constant flow rate of 1 gpm (corresponding to $6.3\times10^{-5}$ $m^3/s$ and $Re = 535$). Samples of the wax-oil gel deposit were collected from

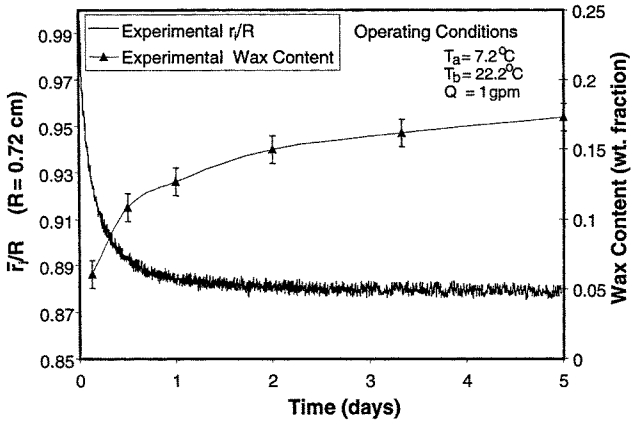


**Figure 6. Internal radius and the wax content of the flow loop deposit as a function of time.**

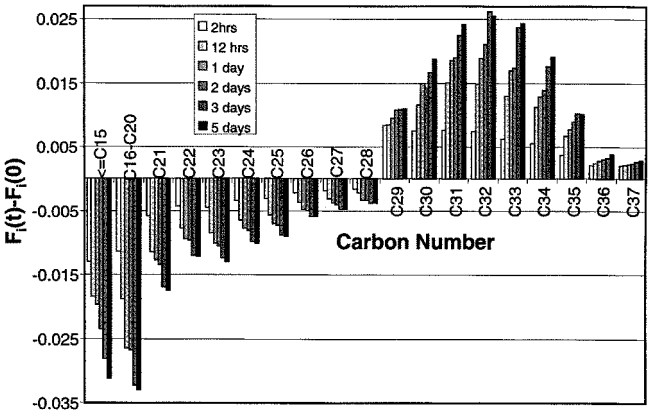


**Figure 8. Changes in carbon number distribution of gel deposits from the flow loop with times.**

the wall of the tubing after each experiment and were analyzed for the wax content. Figure 6 shows the trajectories of the average internal radius (average radius available for flow) and the wax content of the deposit during a flow loop experiment. The operating conditions of the experiment are shown in the figure. It is observed that while the growth of the deposit virtually stops after a day, the wax content of the deposit continues to increase. The deposited gel acts as an insulator to the radial heat transfer. As the deposit thickness grows, the insulating effect increases, and the driving force for further deposition significantly diminishes. Hence, there is virtually no further increase in the film thickness.

### *Aging mechanisms of the gel deposit*

Although the film thickness stops growing, there is still a thermal gradient across the deposit. This gradient may result in an internal mass flux, which in turn may cause the wax content of the gel to continue to increase. The increase in the wax content of the gel deposit with time, that is, aging process, leads to hardening of the deposit. The temperature gradient across the deposit and the mechanical force due to the flow could be responsible for the aging of the gel deposit. The thermal gradient (therefore, the concentration gradient) across the deposit may cause diffusion of the wax molecules into the deposit.

The solubility of the wax in the oil solvent is a strong function of temperature. Therefore, the radial thermal gradient in the pipeline causes a radial concentration gradient of wax, as well as oil. The concentration of wax at the wall of the pipeline is low because of the low wall temperature, as compared to that in the bulk. This concentration gradient leads to the radial diffusion of wax towards the wall of the pipeline. Similarly, the oil diffuses away from the wall due to the concentration gradient of oil. This process is a counterdiffusion of the wax and the oil. The incipient gel deposit is a 3-D matrix of wax crystals having nearly 90–95% oil trapped in it. The wax molecules continue to diffuse into the gel layer, and oil molecules continue to diffuse out until the gel layer hardens with a high wax content (Figure 6).

The samples of the wax-oil gel deposit collected from the wall of the tubing after each experiment, described in the previous subsection, were analyzed using HTGC. The carbon number distributions of the gel samples are shown in Figure 7 along with that of the oil sample.

In order to determine the changes in the carbon number distributions of the gel deposits with time, the distribution of the oil sample is subtracted from those of the gel deposits (Figure 8). It is observed that the mass fractions of hydrocarbons having carbon number greater than 29 increase with time and mass fractions of those having carbon number less than 29 decrease with time. Figure 8 shows that the hydrocarbons having carbon number greater than 29 diffuse into the gel deposit, and those having carbon number less than 29 diffuse out of the gel deposit. Thus, this aging process in the flow loop is a counterdiffusion phenomenon. At the given operating conditions, the *critical carbon number* is 29.

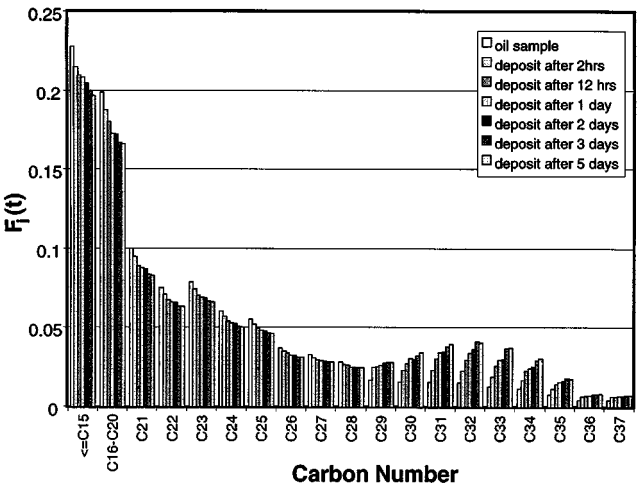


**Figure 7. Carbon number distribution of gel deposits from the flow loop at various times.**

### *Effect of the thermal gradient on aging*

The effect of the temperature difference across the deposit layer on the aging of the deposit was investigated by changing

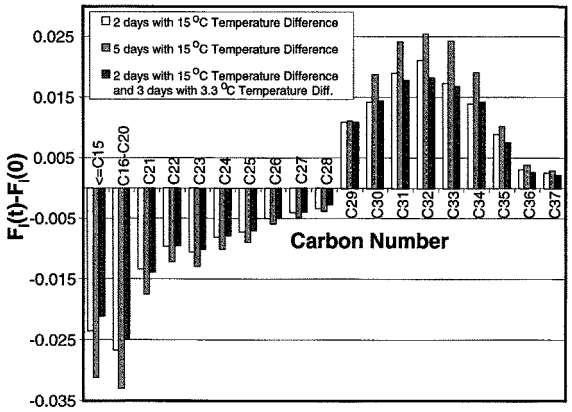


**Figure 9. Changes in carbon number distribution of gel deposits from the flow loop with different temperature differences across the deposit.**

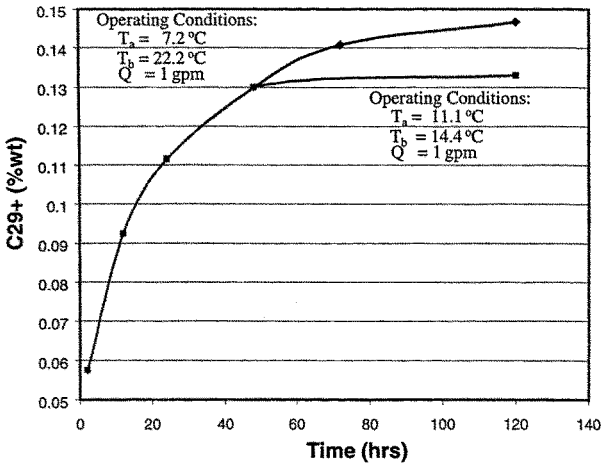


**Figure 10. Mass fraction of the $C29^+$ hydrocarbons of gel deposits from the flow loop with different temperature differences across the deposit.**

the wall temperature and the bulk oil temperature. The flow loop was operated at a bulk oil temperature of 22.2°C and a wall temperature of 7.2°C for two days. After two days, the bulk oil temperature was decreased to 14.4°C (still above the cloud point, 13.9°C), and the wall temperature was increased to 11.1°C; the experiment was continued for three more days. Figure 9 shows that the molecular weight distribution of the gel deposit did not change considerably after two days when the bulk temperature was reduced from 22.2 to 14.4°C, although the weight fraction of waxes considerably increases after two days if the bulk temperature was kept 22.2°C. In Figure 10, the mass fractions of all the hydrocarbon having carbon numbers greater than 29 are shown as a function of time. It can be seen that, as long as there is a considerable temperature difference (15°C) across the deposit layer, the C29+ fraction increases with time, but when the temperature difference was decreased to 3.3°C, the C29+ fraction remains virtually constant. This result shows that the aging rate of the gel deposit significantly decreases when the temperature difference across the gel deposit is reduced from 15°C to 3.3°C, even though the oil continued to flow over the gel deposit for three days. These results indicate that the aging of the deposit is a strong function of the temperature difference across the deposit.

### *Effect of the mechanical compression on aging*

The surface of the deposited gel is rough in nature. Hence, it is expected that the fluid flow over the gel surface will not exert a shear force, but also a compressive force on the gel deposit (Figure 11). This compressive force could squeeze the oil out of the gel deposit and make it harder with time. It can be noted from Figure 10 that the aging rate of the gel deposit essentially vanishes when the temperature difference across the gel deposit is reduced from 15°C to 3.3°C, even though the oil continues to flow over the gel deposit for three more days, under the same pressure. This result indicates that the aging process is a much weaker function of the compressive force than of the temperature difference across the deposit.

The above analysis of the flow loop experiments clearly shows that the temperature gradient across the gel deposit, which leads to the counterdiffusion of the wax and oil

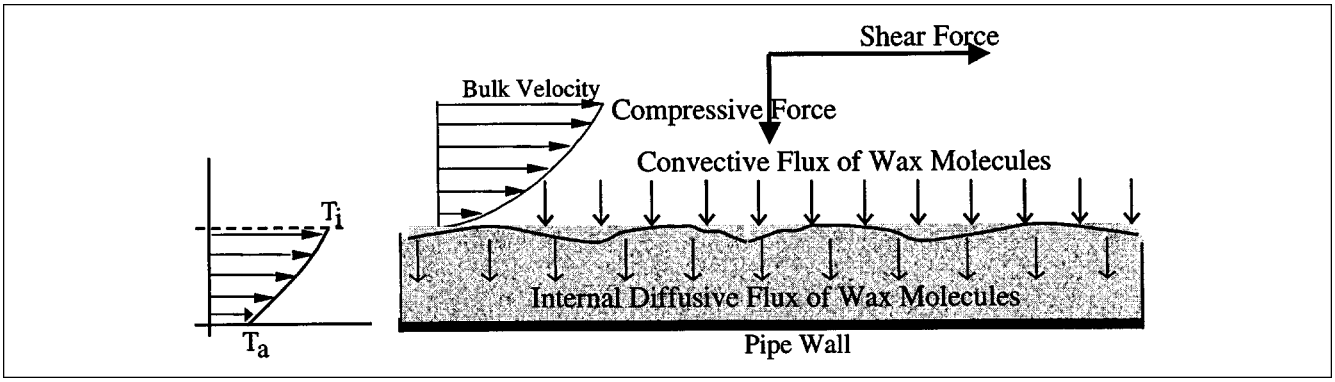


**Figure 11. Wax-oil deposition on the pipe-wall showing forces on the gel deposit exerted by the flow of the wax-oil mixture.**

molecules into and out of the gel deposit, is the prime cause of aging.

## Development of the Model

Figure 11 shows the wax-oil gel deposition on the pipe wall. At any instance, there is a radial convective flux of wax molecules towards the gel layer. A diffusive flux of wax molecules into the gel layer is also present, resulting in continuous addition of the wax molecules to the gel layer, thereby increasing its wax content. It is assumed that the overall wax content of the gel layer is only a function of time and axial location, and does not vary radially because of the thinness of the deposit.

### *Assumptions*

(1) The dominant mechanism of the wax deposition is molecular diffusion; particulate deposition mechanisms such as particle diffusion and gravity settling are neglected.

(2) The extent of shear removal of the gel deposited in the flow loop is negligible.

(3) All processes are assumed to be quasi-steady state.

(4) Heat transfer from the oil-gel interface to the cold pipe-wall is a one-dimensional heat transfer.

(5) There is no radial variation in the wax content of the thin gel deposit.

(6) The thermal conductivity of the gel is a function of its wax content.

Experimental verification and the validity of these assumptions will be discussed in the following section.

### *Verification of the assumption*

Various mechanisms such as particulate deposition and shear removal have been discussed in the wax deposition literature along with the molecular diffusion mechanism. In this section, results from flow loop experiments will be discussed and the extent to which these mechanisms affect the deposition process will be verified.

*Particulate Deposition.* The particulate deposition mechanism was quantified using flow loop experiments. The following experimental conditions are required to determine the extent of particulate deposition.

(1) Wax particles have to be present in the bulk fluid inside the flow loop. Consequently, the bulk temperature has to be below the cloud point.

(2) There should be no molecular diffusion of wax in the system. This condition was achieved by keeping the bulk oil temperature equal to the wall temperature of the flow loop, thus assuring no radial temperature gradient.

(3) It is possible that the wax particles may not stick to the steel wall. Hence, a thin layer of wax was deposited in the test section of the flow loop before investigating the particulate deposition.

Initially, a wax-oil gel was deposited with oil flowing at the rate, $Q = 7$ gal/min ($4.41 \times 10^{-4}$ m$^3$/s). The bulk oil temperature was $T_b = 30.6$°C, and the wall temperature was maintained at $T_a = 17.8$°C. The deposition was done for 12 h. After initial deposition, the bulk oil sample was cooled down to the wall temperature 17.8°C. As soon as the temperature of the bulk oil sample decreased below the cloud point, wax particles appeared in the bulk oil sample. Then, particulate flow was started at a flow rate of 1 gal/min ($6.3 \times 10^{-5}$ m$^3$/s and $Re = 1{,}200$). From the pressure drop in the reference section and the test section, the initial thickness was calculated to be $\delta_{\text{final}} = 0.31\ R_o$. The thickness of the deposited layer was observed to remain a constant even after the particulate flow was started, as shown in Figure 12, that is, the initial thickness was preserved. Thus, in this case, it was observed that there was no particle deposition.

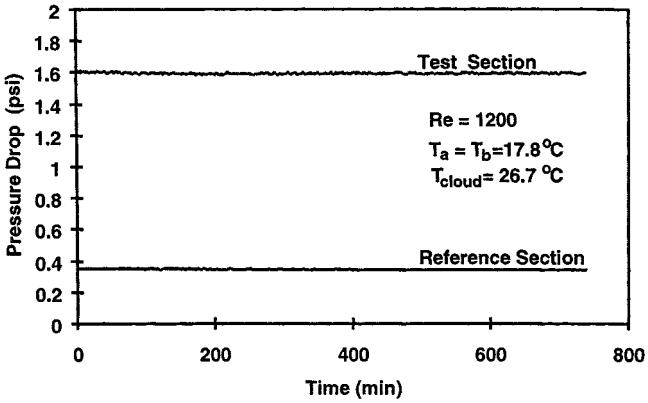


**Figure 12. Pressure drop in the reference and test section during the flow of the oil below the cloud point at a Reynolds number of 1,200.**

*Shear Removal.* The gel deposit is subjected to shear forces due to the flow of the oil (Figure 11). If the shear force exerted on the deposit were higher than the cohesive/adhesive forces within the gel, then this shear would cause part of the gel deposit to break free.

A flow loop experiment, similar to the one described in the previous subsection, was carried out to study the effect of the flow rate on sloughing. Again, a wax-oil gel was deposited initially, with the same operating conditions as in the previous experiment, except that this time the deposition was done for 17 h. After initial deposition, the bulk oil sample was cooled down to the wall temperature 17.8°C. Then, particulate flow was started at a flow rate of 5 gpm (corresponds to $3.15 \times 10^{-4}$ m$^3$/s and $Re = 5{,}200$).

The initial deposit thickness, in this case, was $\delta_{\text{initial}} = 0.35\ R_o$. In this case, it was observed that there was no particle deposition, although, a small extent of sloughing of the initial deposited layer was observed with time, as shown in Figure 13. The final thickness after 8 h of particulate flow was calculated to be $\delta_{\text{final}} = 0.34\ R_o$.

From the above experimental results (as shown in Figures 12 and 13), it can be concluded that the assumption of particulate deposition being negligible is valid. Although a very small amount of sloughing of the wax-oil gel was observed in the case where the Reynolds number was equal to 5,200, the assumption of no sloughing is valid for the operating conditions of flow loop experiments, because Reynolds number was less than 2,100 for all of the experiments.

The quasi-steady-state approximation assumes that heat transfer is instantaneous. Also, the axial heat transfer is neglected. These assumptions are reasonable in the range of

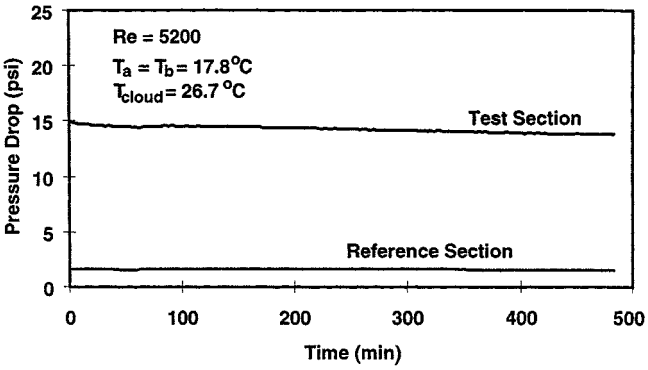


**Figure 13. Pressure drop in the reference and test section during the flow of the oil below the cloud point at an average Reynolds number of 5,200.**

the given experimental conditions and simplify the mathematics. The assumption that there is no radial variation of the wax content in the deposit holds due to the thinness of the gel deposits that are studied. The final assumption is that thermal conductivity of the gel is a function of its wax content. This has been observed experimentally and has also been reported in the literature (Carslaw and Jaeger, 1959).

### *Mass balance*

The radial temperature gradient inside the pipe, where the wall temperature is lower than the cloud point temperature, gives rise to a radial gradient of wax concentration in the oil, inasmuch as the wax concentration depends on the temperature. The wax concentration in the liquid at the centerline is higher than the wax concentration in the liquid at the wall owing to the higher centerline temperature. This concentration gradient leads to a radial convective flux of wax molecules towards the wall. This flux is determined by the difference in the wax concentration between the bulk and the interface of the oil and the gel layer. Mass balance gives the following equation

$$\text{Rate of change of wax in the gel deposit} = \text{Radial convective flux of wax molecules from the bulk to the fluid–gel interface}$$

$$\frac{d}{dt}\left[\pi\left(R^2 - r_i^2\right)\bar{F}_w(t)\,L\,\rho_{\text{gel}}\right] = 2\pi r_i L k_l\left[C_{wb} - C_{ws}(T_i)\right]$$

The density (kg/m$^3$) of the gel $\rho_{\text{gel}}$ is a constant and does not vary with time, because the densities of the oil and the wax are equal. Hence

$$\pi\left(R^2 - r_i^2\right)\frac{d\bar{F}_w(t)}{dt} - 2\pi r_i \bar{F}_w(t)\frac{dr_i}{dt} = \frac{2\pi r_i k_l}{\rho_{\text{gel}}}\left[C_{wb} - C_{ws}(T_i)\right]$$

After transforming the radius (m) $r_i$ to a dimensionless measure of the thickness of the wax deposit $y = (1 - r_i/R)$, we obtain

$$\frac{y}{(1-y)}\left(1 - \frac{y}{2}\right)\frac{d\bar{F}_w(t)}{dt} + \bar{F}_w(t)\frac{dy}{dt} = \frac{k_l}{\rho_{\text{gel}} R}\left[C_{wb} - C_{ws}(T_i)\right] \quad (1)$$

### *Growth rate of the gel deposit*

In addition to the convective mass flux of wax molecules from the bulk to the interface, there is also an internal diffusion process. There is a temperature gradient across the gel layer; hence, there is an internal diffusive flux of wax molecules within the gel deposit. The rate of deposition of wax is a sum of two quantities: the rate of increase of the thickness of the deposit and the rate of increase in the wax content of the deposit. The latter is the result of the internal diffusion. Hence, the rate of increase of the thickness of the deposit (equivalently, the rate of decrease of the radius available for the flow of oil) can be obtained as

$$\text{Rate of addition of wax in growing the gel deposit} = \text{Radial convective flux of wax molecules from the bulk to the fluid–gel interface} - \text{Diffusive flux into the gel at the gel interface}$$

$$-2\pi r_i \bar{F}_w(t)\rho_{\text{gel}}\frac{dr_i}{dt} = 2\pi r_i k_l\left[C_{wb} - C_{ws}(T_i)\right] - 2\pi r_i\left(-D_e\left.\frac{dC_w}{dr}\right|_i\right)$$

Substituting in terms of $y$

$$\bar{F}_w(t)\rho_{\text{gel}}\frac{dy}{dt} = \frac{k_l}{R}\left[C_{wb} - C_{ws}(T_i)\right] + \frac{D_e}{R}\frac{dC_{ws}}{dT}\left.\frac{dT}{dr}\right|_i \quad (2)$$

### *Energy balance*

The rate at which heat is conducted across the thickness of the deposit is a sum of the radial convective heat flux and the latent heat of solidification. Hence, the energy balance equation is

$$\text{Radial convective heat flux from the bulk to the interface} = \text{Rate of heat conduction through the deposit} - \text{Latent heat of solidification}$$

$$2\pi r_i h_i(T_b - T_i) = \frac{2\pi k_e(T_i - T_a)}{\ln(R/r_i)} - 2\pi r_i k_l\left[C_{wb} - C_{ws}(T_i)\right]\Delta H_f$$

Rearrangement gives

$$T_i = \frac{h_i T_b + \left( \frac{k_e/R}{-(1-y)\ln(1-y)} \right) T_a + k_l \left[ C_{wb} - C_w(T_i) \right] \Delta H_f}{h_i + \left( \frac{k_e/R}{-(1-y)\ln(1-y)} \right)} \tag{3}$$

Assuming no variation of the thermal conductivity of the gel deposit with radial direction, the temperature gradient at the gel interface is given by

$$\left. \frac{dT}{dr} \right|_i = \frac{(T_i - T_a)}{R(1-y)\ln(1-y)} \tag{4}$$

### *Overall mass balance*

The wax concentration in the bulk oil $C_{wb}$ (kg/m$^3$) continuously changes with time due to the depletion of wax content of the bulk oil as the wax-oil gel deposits on the wall. The overall mass balance is as follows

$$\text{Change in the wax content of the bulk oil} = \text{Total amount of wax deposited as gel}$$

$$V_R(C_{wbo} - C_{wb}) = \int_0^L \pi R^2 y(2-y) \bar{F}_w \rho_{\text{gel}} \, dL$$

Rearrangement gives

$$C_{wb} = C_{wbo} - \int_0^L \frac{\pi R^2 y(2-y) \bar{F}_w \rho_{\text{gel}}}{V_R} dL \tag{5}$$

Initial Condition

$$\text{At time } t = 0,\ y = 0 \text{ and } \bar{F}_w = C_{wbo}.$$

### *Parameter values*

*Correlations for the Transfer Coefficients $h_h$ and $k_l$.* For laminar flow in a pipe, the heat-transfer coefficient can be obtained from the empirical correlations described below. The Hausen correlation is valid for long distances from the inlet, and the Seider and Tate correlation is valid for short tubes. The actual correlations in the literature for a length-averaged value of the Nusselt number have been converted to obtain the local value of the Nusselt number. The analogy between heat transfer and mass transfer has been used to obtain the value of the mass-transfer coefficient

Hausen Correlation (Hausen, 1943)

$$Nu_i = 3.66 + 1.7813 \times 10^{-3} \times \left( \frac{(Gz_i)^{(5/3)}}{\left(1 + 0.04 \times (Gz_i)^{(2/3)}\right)^2} \right) \quad \text{for } Gz_i < 100 \tag{6}$$

Seider and Tate Correlation (Seider and Tate, 1936)

$$Nu_i = 1.24 \times (Gz_i)^{(1/3)}, \quad \text{for } Gz_i > 100 \quad \text{here } i = h \text{ for heat transfer and } i = m \text{ for mass transfer} \tag{7}$$

Heat transfer coefficient

$$h_h = \frac{Nu_h \times k_{\text{oil}}}{2R}$$

Mass transfer coefficient

$$k_l = \frac{Nu_m \times D_{wo}}{2R}$$

*Thermal Conductivity of the Gel Deposit.* The thermal conductivity of the gel deposit is assumed to be a function of its wax content. The following Maxwell correlation (Carslaw and Jaeger, 1959) was used to calculate the thermal conductivity of the gel

$$k_{\text{dep}} = \frac{\left[2k_{\text{wax}} + k_{\text{oil}} + (k_{\text{wax}} - k_{\text{oil}})\bar{F}_w\right]}{\left[2k_{\text{wax}} + k_{\text{oil}} - 2(k_{\text{wax}} - k_{\text{oil}})\bar{F}_w\right]} k_{\text{oil}} \tag{8}$$

*Molecular Diffusivity.* Molecular diffusivity of wax in oil can be obtained from correlations. The calculation of the molecular diffusivity is shown in the appendix.

*Solubility of Wax in the Oil Solvent.* The solubility of wax in the oil solvent $C_{ws}$ (kg/m$^3$) is a strong function of temperature. The solubility decreases rapidly with decrease in the temperature of the solution. For a typical wax-oil sample, the solubility can be expressed as

$$C_{ws}(T_i) = a(T_i + b)^c \tag{9}$$

and the derivative of the solubility with temperature is given by

$$\frac{dC_{ws}}{dT_i} = ac(T_i + b)^{c-1} \tag{10}$$

where $T_i$ is in °C. For the particular wax-oil mixture used in this study, $a$, $b$, and $c$ are $4.9 \times 10^{-9}$ kg/m$^3$·K$^6$, 17.8°C, and 6, respectively.

*Effective Diffusivity of Wax Molecules into the Gel.* The effective diffusivity of the wax molecules into the gel deposit is a function of porosity of the gel. It is assumed that the average aspect ratio of the wax crystals is $\alpha$. Hence, the following expression (Cussler et al., 1988), derived for porous media of flake-like particles, is used for the effective diffusivity

$$D_e = \frac{D_{wo}}{1 + \alpha^2 \bar{F}_w^2 / (1 - \bar{F}_w)} \tag{11}$$

It is assumed that the aspect ratio of the wax crystals varies linearly with the wax content of the gel deposit.

### *Computational procedure*

The coupled differential equations (Eqs. 1 and 2), (the mass balance and internal diffusion (aging) equations) were solved numerically to obtain the profiles and the time trajectories of the thickness and the solid wax content of the gel.

A closed system, where a fixed amount of oil recirculates through the pipe, was considered, so as to simulate the laboratory flow loop. Here, the inlet temperature $T_b$ is assumed to be a constant by suitably using a reservoir maintained at that temperature. However, the bulk concentration of the wax would deplete with time, as the wax-oil gel deposits.

Because the thickness and wax content of the deposit vary down the length of the pipe as well as with time, the integrations have to be performed with respect to both length and time. The length of the pipe was divided into 50 equal grids. The deposition rate is expected to be fast initially and then slow down, inasmuch as there is a larger driving force initially. Hence, initially very small time steps were used ($\Delta t = 30$ s, for $t < 10$ min), and then progressively bigger time steps were used ($\Delta t = 2$ min, for 10 min $< t <$ 1 h, and $\Delta t = 10$ min, thereafter). This numerical scheme was tested for convergence and stability and found to be robust.

The coupled differential equations were solved throughout the length of the pipe at each time instant using Runge-Kutta algorithms. In order to solve these equations, the values of the interfacial temperature $T_i$, the gradient of the interfacial temperature (°C) $dT_i/dr$, and the liquid wax concentration $C_{ws}(T_i)$, as well as the temperature derivative of the wax concentration $dC_{ws}/dT$ at the interface, were required. $C_{ws}(T_i)$ and $dC_{ws}/dT$ were obtained from Eqs. 9 and 10. The interfacial temperature $T_i$ was obtained from the energy balance equation (Eq. 3); $dT_i/dr$ is obtained from Eq. 4. It should be noted that the algebraic Eqs. 3 and 4 are also coupled, that is, the value of $T_i$ has to be known to calculate $C_{ws}(T_i)$ and vice versa. Hence, an iterative procedure has to be used to solve these equations simultaneously.

Solving the entire system of equations at a particular time instant gives the *profiles* of thickness and wax content at that instant. With these profiles as initial values, the equations were again solved at the next time instant. This procedure was repeated up to $t = 5$ days. Thus, the *trajectories* of thickness and wax content are obtained at each location.

## Results and Discussion

### *Buildup of the incipient gel layer*

The following subsections discuss the formation and the structure of the incipient gel layer.

*Structure of Multicomponent Wax Crystals.* Petroleum waxes are multicomponent mixtures of high molecular weight saturated hydrocarbons, predominantly paraffins, in the range of $C_{18} - C_{65}$ (Srivastava et al., 1993). A multicomponent wax crystal is a solid solution with a lamellar structure similar to pure *n*-alkanes with orthorhombic subcells (Clavell-Grunbaum et al., 1997). Diffraction techniques have usually been employed to determine these structures because these techniques are sensitive to crystal order (Dorset, 1991; Dorset and Snyder, 1996). Wide-angle reflections provide lateral unit cell dimensions of the crystal and reveal the type of lateral cell packing.

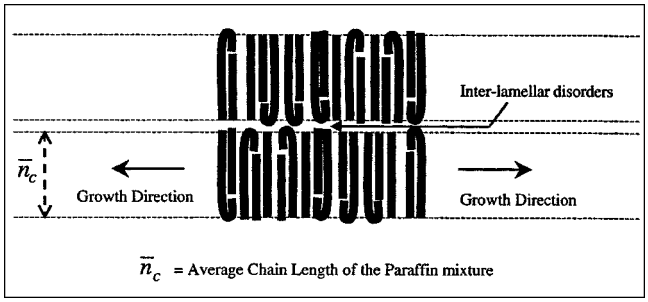


**Figure 14. Lamellar structure of the multicomponent wax crystal.**

X-ray diffraction analysis shows that a single packing layer of a multicomponent paraffin wax crystal has a thickness equal to the average length of the wax molecules in the mixture, as shown in Figure 14 (Dirand et al., 1998). A wax molecule with a carbon number greater than the average carbon number bends to insert itself inside the layer, and associates itself with a molecule with a carbon number lower than the average (c.f. Figure 14). The mismatch between the length of the molecules and the thickness of the packing layer causes conformational disorders in the interlamellar regions of these crystals. These interlamellar disorders impart to these crystals their wax-like properties (Clavell-Grunbaum et al., 1997).

*Structure of the Incipient Gel.* When a wax-oil mixture is cooled, as soon as the temperature drops below the cloud point, wax molecules start precipitating out of the solution in the form of orthorhombic subcrystals that combine to form the lamellar structures (that is, sheet-like morphology). As the mixture is cooled further, the 2-D lateral growth of these sheet-like crystals (c.f. Figure 14) results in the formation of thin flakes. The growth of these sheet-like crystals in the third dimension may be hindered by the conformational disorders at the interlamellar regions. When the size and density of these flakes reach a critical value where they overlap and interlock with each other, the entire wax-oil solution forms a gel (Holder and Winkler, 1965a). This critical value would depend on the shear and thermal histories of the mixture, as well as the composition of the mixture. For crude oils which contain more than 10 wt. % of *n*-paraffins, under static conditions, the gelation of the crude oil can take place when approximately 2 wt. % of waxes have precipitated out in the solution (Létoffé et al., 1995). However, under flow conditions, the weight fraction of the precipitated wax in the incipient gel is a strong function of the shear and thermal histories of the mixture (Singh et al., 1999). The incipient gel of the wax-oil mixture is also similar to the gelation of sheet-like kaolinite particles in the aqueous solution (Pierre et al., 1995).

### *Effect of operating conditions on the rate of deposition*

In order to understand the effect of the flow rate on the deposition process, a series of gel deposition experiments were conducted in the laboratory flow loop at various flow rates in the laminar regime. An oil sample having wax (0.67

**Table 1. Parameters Fixed for all the Cases under Study**

| Parameter | Value |
|---|---|
| Length of the pipe, $L$ | 8 ft (2.44 m) |
| Inner radius of the pipe, $R$ | 0.72 cm |
| Volume of the reservoir, $V_R$ | 8 gal (0.03 $m^3$) |
| Inlet temperature of the oil, $T_b$ | 22.2°C |
| Run time — | 5 d |

wt. %) at a temperature 22.2°C was flown through the flow loop at flow rates 1 gpm (that is, $6.3\times10^{-5}$ $m^3/s$), 2.5 gpm, and 4 gpm (corresponding to $Re = 535$, 1,338 and 2,140, respectively). Table 1 shows the values of the parameters that were constant for all the experiments. The wall of the tubing was kept constant at 8.3°C and the gel deposition was monitored with time. Figure 15 shows the average internal radius of the tubing as a function of time during wax deposition for the three different flow rates. In all three cases the growth of the wax deposit virtually stops after a certain period of time. This condition arises as a result of the insulating effect of the wax deposit, that is, the thermal resistance of the wax deposit is sufficient to prevent further deposition in the flow loop. However, the deposit may continue to grow in an actual subsea pipeline over long periods of time until the pipeline is essentially plugged. The final average thickness of the deposit is smaller for a higher flow rate. Figure 16 shows the trajectories of the interfacial temperature for these three flow rates. For a higher flow rate, the rate of heat transfer is higher; hence, the rate of increase of the interface temperature is higher. For all the three flow rates, the interface temperature rapidly approaches the cloud point temperature 13.9°C, which is independent of the flow rate. Figures 15 and 16 show a similarity between the thickness and interface temperature trajectories: both increase very fast initially, and then level off. When the interface temperature approaches the cloud point after the initial rapid increase, the gel thickness virtually stops growing because the driving force is then negligible. For a higher flow rate, the interface temperature approaches the cloud point in a shorter period of time. Hence, the gel deposit has a shorter time of growth in thickness. Also,

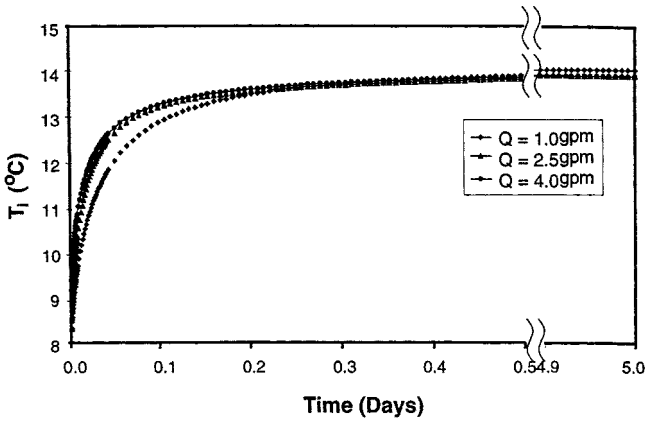


**Figure 16. Interface temperature as a function of time for various flow rates at the mid-section of the flow loop.**

the faster the interface temperature approaches the cloud point, the slower is the rate of growth of the deposit. Hence, for a higher flow rate, the gel deposit is thinner.

The effect of the wall temperature on the aging of the wax deposit was investigated by performing a series of flow loop experiments at various well temperatures. An oil sample having wax (0.67 wt. %) at a temperature of 22.2°C was flown through the flow loop with wall temperatures 4.4°C, 7.2°C, and 8.3°C at a constant flow rate of 1 gpm (corresponding to $6.3\times10^{-5}$ $m^3/s$ and $Re = 535$). Figure 17 shows the average internal radius of the tubing as a function of time during wax deposition for the three wall temperatures. Again, it is observed that in all three cases the growth of the wax deposit virtually stops after a certain period of time. It can be seen that the final thickness of the deposit is smaller for a higher wall temperature. Figure 18 shows the interface temperature trajectories for these three wall temperatures. Again, the similarity between the thickness and the interface temperature trajectories is to be noted. For a higher wall temperature, the cloud point is reached in a shorter period of time, resulting in a thinner deposit.

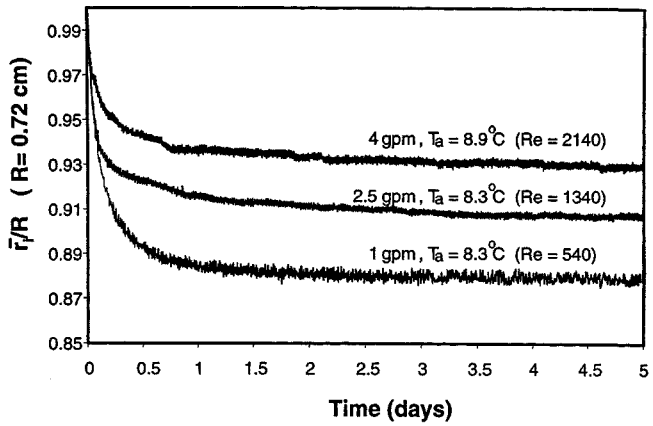


**Figure 15. Average internal radius of the flow loop tubing as a function of time for various flow rates.**

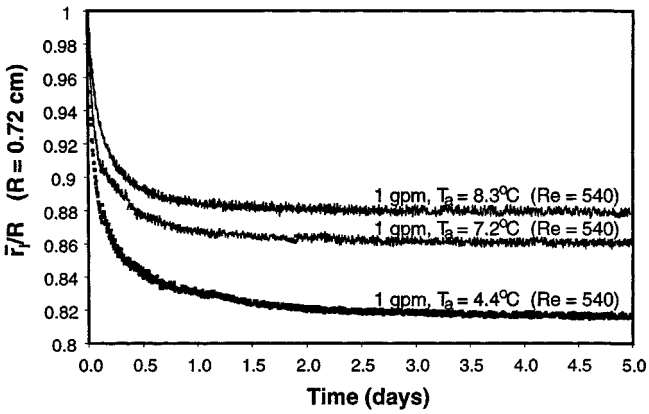


**Figure 17. Average internal radius of the flow loop tubing as a function of time for various wall temperatures.**

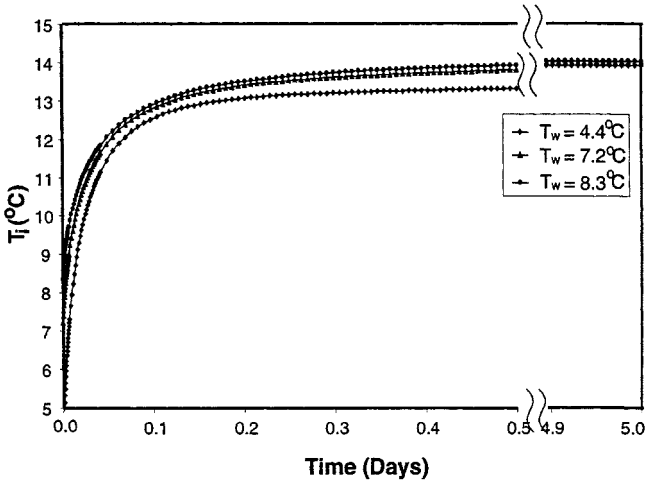


**Figure 18. Interface temperature as a function of time for various wall temperatures at the mid-section of the flow loop.**

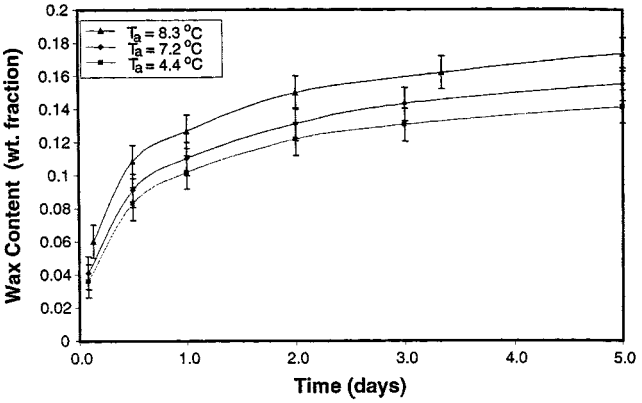


**Figure 20. Wax content of the gel deposit as a function of time for various wall temperatures.**

*Effect of operating conditions on the rate of aging*

To study the effect of the operating conditions, that is, the flow rate and the wall temperature on the rate of aging of the gel, the gel deposits collected from the experiments described in the previous section were analyzed for their wax contents using HTGC. Figure 19 shows the wax content of the gel deposits as a function of time for the three flow rates. The rate of increase of the wax content is higher for higher flow rates. Figure 20 shows the wax content of the gel deposits as a function of time for the three wall temperatures. The rate of increase of the wax content is higher for higher wall temperatures.

From Figures 15 and 19, as well as Figures 17 and 20, it can be seen that the thicker the deposit, the lower the wax content of the deposit and vice versa. For example, a higher flow rate (or a higher wall temperature) leads to a smaller thickness and a higher wax content of the deposit. This result may be attributed to the fact that a lower thickness results in a higher temperature gradient across the gel, resulting in a higher diffusive flux of wax inside the gel, leading to a higher solid wax fraction in the gel.

*Radial temperature profiles for various operating conditions*

Figure 21 shows the variation of temperature along the radial direction for various flow rates inside the flow loop tubing at a constant wall temperature of 8.3°C. The temperature at the interface of the oil and the deposit in all of these cases is the cloud point (13.9°C). For higher flow rates, the thickness of the deposit, as well as the thermal boundary thickness, is smaller, which results in a higher thermal gradient across the deposit. The higher thermal gradient causes the deposit to age faster at higher flow rates.

Figure 22 shows the variation of temperature along the radial direction for various wall temperatures at a constant flow rate of 1 gpm ($6.3\times10^{-5}$ $m^3/s$). The boundary layer thickness is nearly the same for all these cases. However, for a higher wall temperature, the deposit thickness is lower, which results in a higher thermal gradient across the deposit, leading to a higher aging rate.

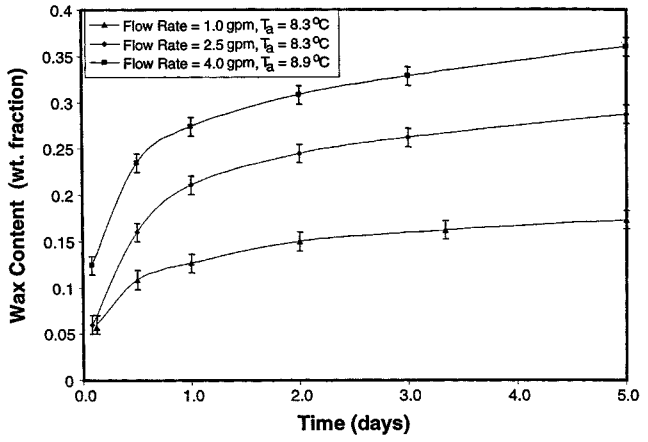


**Figure 19. Wax content of the gel deposit as a function of time for various flow rates.**

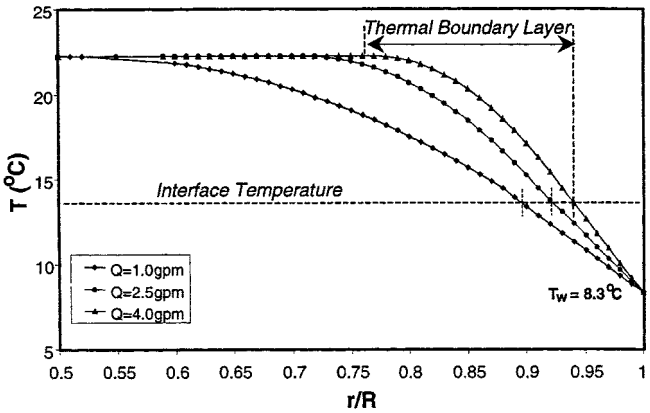


**Figure 21. Radial temperature profiles for various flow rates at the mid-section of the flow loop.**

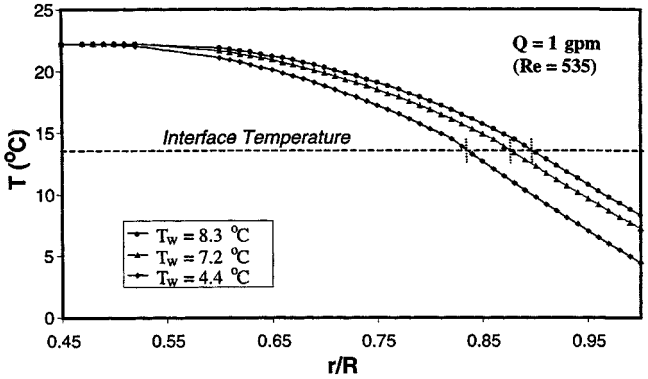


**Figure 22. Radial temperature profiles for various wall temperatures at the mid-section of the flow loop.**

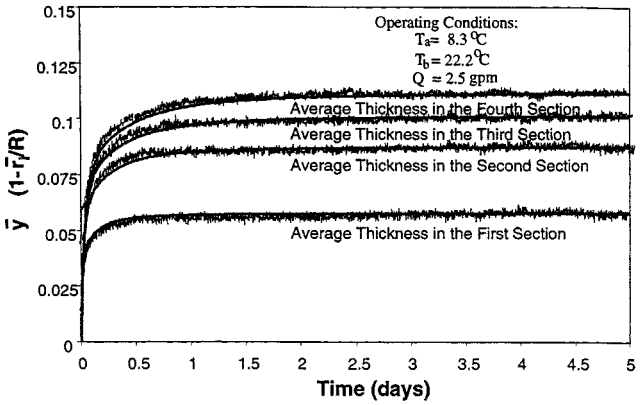


**Figure 24. Trajectories of average gel thicknesses for various sections of the flow loop.**

## Theory vs. Experiments

Three different wall temperatures (at a fixed flow rate) and three different flow rates (at a fixed wall temperature) were studied, the details of which have been specified in the previous section. The mathematical model discussed previously was used to predict the experimental data. The data from the flow loop experiments and the corresponding theoretical predictions are compared and discussed in the following section. The aspect ratio of the wax crystals was used to match the theoretical and experimental values.

### *Axial variation of gel thickness*

The gel deposit thickness is not uniform all along the length of the flow loop, because of the variation of the rates of heat and mass transfer along the length. The experimental results discussed previously show the average thickness along the length of the flow loop. This thickness was calculated from the total pressure drop across the entire test section. Five pressure taps were installed along the length of the test section (c.f. Figure 5), enabling the measurement of the differential pressure across four subsections of the test section. From the measurements, the average thickness along each of these subsections can be calculated.

The simulation results provide the thickness profiles at various times. These are shown in Figure 23. As seen from the figure, the thickness increases along the length of the flow loop at large times. From this data, the average thickness for each subsection can be calculated, and plotted as a function of time. Figure 24 shows the comparison of the experimentally observed thickness trajectories with the simulation results.

### *Variation of flow rate*

Figures 25, 26 and 27 show comparisons of the experimental and theoretically predicted trajectories of the thickness and the wax content of the deposit for the three different flow rates described previously (at a constant wall temperature). For the case illustrated in Figure 25, the average aspect ratio of the wax crystals was assumed to vary linearly with the wax content of the deposit, from a value of 1 to 24. For the case of Figure 26, the aspect ratio was varied between 1 to 14, whereas, for the case of Figure 27, it was var-

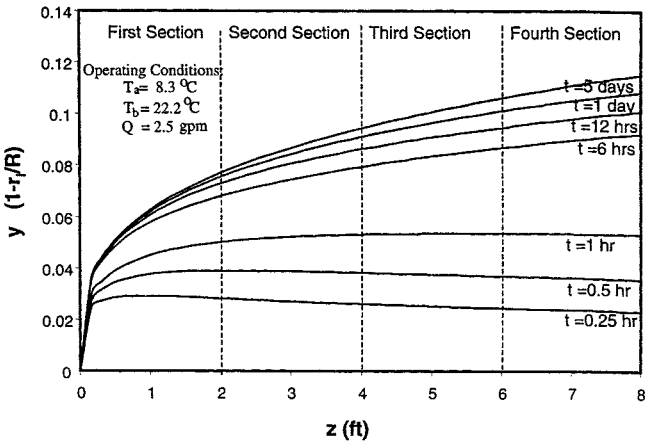


**Figure 23. Dimensionless thickness profiles for various times.**

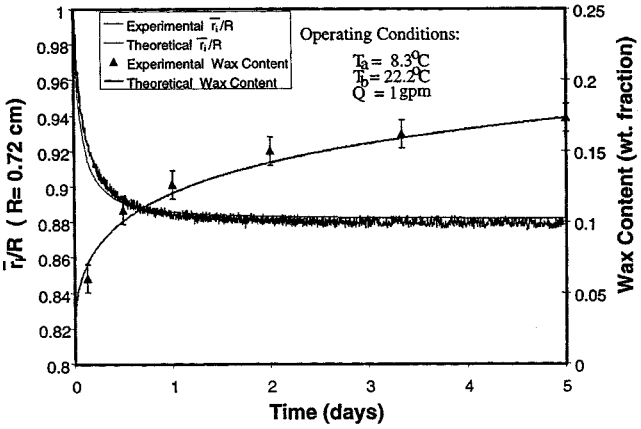


**Figure 25. Theory vs. experiment for the wax deposition under a flow rate of 1 gal/min (0.06 L/s) and wall temperature of 8.3°C.**

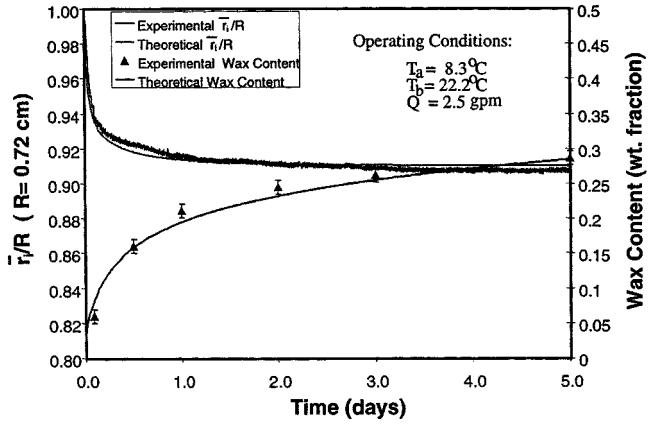


**Figure 26. Theory vs. experiment for the wax deposition under a flow rate of 2.5 gal/min (0.16 L/s) and wall temperature of 8.3°C.**

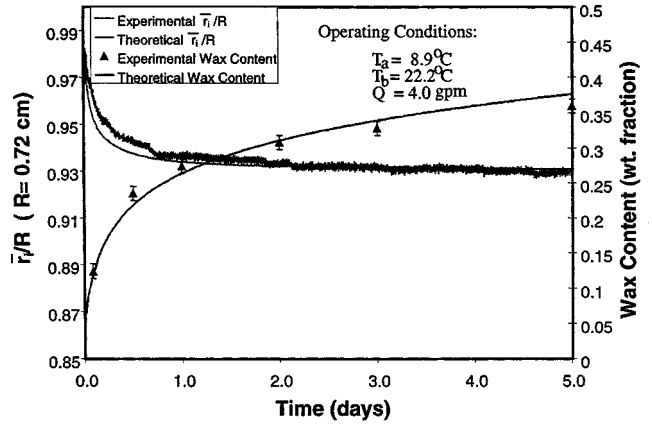


**Figure 27. Theory vs. experiment for the wax deposition under a flow rate of 4 gal/min (0.25 L/s) and wall temperature of 8.9°C.**

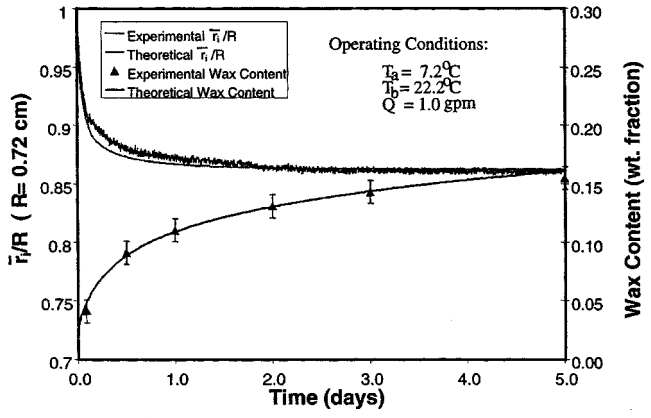


**Figure 28. Theory vs. experiment for the wax deposition under a flow rate of 1 gal/min (0.06 L/s) and wall temperature of 7.2°C.**

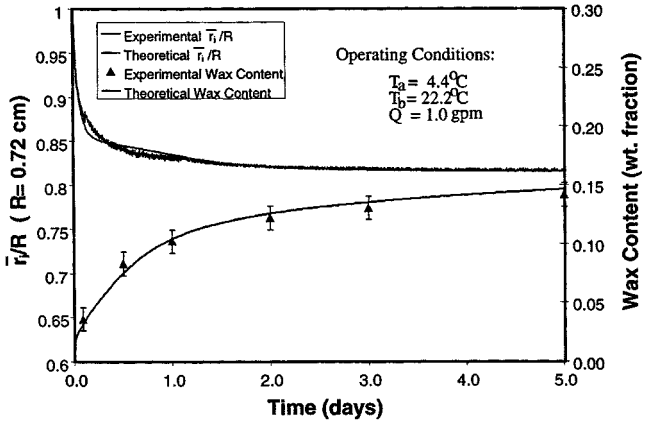


**Figure 29. Theory vs. experiment for the wax deposition under a flow rate of 1 gal/min (0.06 L/s) and wall temperature of 4.4°C.**

ied from 1 to 10. There is an excellent match between theory and experiment for all the three cases, as seen in the figures.

### *Variation of wall temperature*

Figures 25, 28 and 29 show the comparisons between theory and experiment of the three wall temperatures described previously, with the same flow rate of 1 gpm (that is, $6.3 \times 10^{-5}$ $m^3/s$). For all these three cases, the aspect ratio had the same linear variation with the wax content of the deposit. Again, these figures show the excellent agreement between theoretical predictions and experimental data.

### *Aspect ratio of the wax particles*

The effective diffusion of the wax molecules inside the wax-oil gel is a function of the average aspect ratio of the wax particles in the gel phase (Eq. 3). To predict the experimental data using the mathematical model, the aspect ratio had to be varied with the operating conditions. Figure 30 shows the average aspect ratio of the wax particles as a function of the

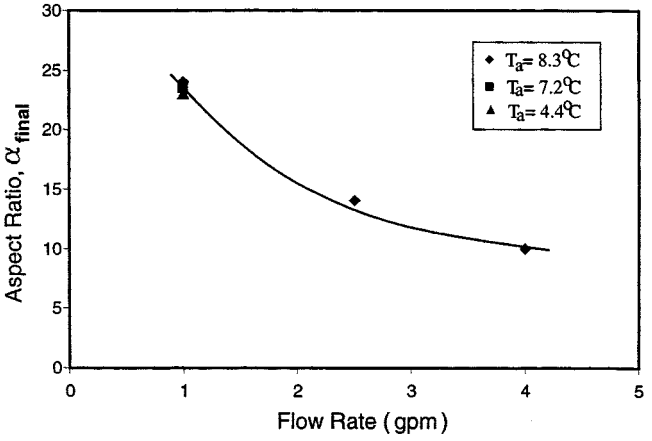


**Figure 30. Final aspect ratio of the wax crystals in the gel deposit as a function of the flow rate and wall temperature.**

flow rate. It is observed that the aspect ratio of the wax particles decreases with the flow rate of the bulk oil. However, it is a much weaker function of the wall temperature. This result implies that, during the deposition of the wax-oil gels under flow conditions, the shear stress applied on the gel alters the morphology of the gel crystals by reducing the aspect ratio of the crystals in the gel.

## Conclusions

High molecular weight paraffins form stable crystals at low temperature due to the low solubility of these compounds in aromatic or naphthenic solvents. This crystallization of paraffins leads to the formation of gels of very complex morphology. A model system of wax and oil was used to understand the gelation process of these mixtures. The incipient wax-oil gel deposited on the wall of the flow loop has a significant amount of oil trapped in the 3-D network structure of the wax crystals. As a result, the gel behaves as a porous medium in which wax molecules continue to diffuse and the wax content of the deposited gel increases with time.

A series of laboratory flow loop experiments were carried out for various lengths of time to elucidate physics of the aging process of the gel deposit. The deposited gels collected from these experiments were analyzed and the wax content of the gel was found to be a strong function of the aging time. It was observed that the aging of the gel deposit is a strong function of the temperature difference across it. The aging was found to be a counterdiffusion phenomenon in which wax molecules diffuse into the gel deposit and oil molecules diffuse out, resulting in the increase in the wax content of the deposit.

A mathematical model was developed to describe the wax deposition process in a laboratory flow loop. The coupled system of differential and algebraic equations of heat and mass transfer inside and outside the gel deposit was solved numerically. An increase in the wall temperature results in a decrease in the gel thickness, and consequently an increase in the wax content of the gel. An increase in the flow rate also has a similar effect—a decrease in the thickness and an increase in the solid wax fraction. The incipient wax content of the gel was found to vary with the flow rate and the wall temperature. As the flow rate increases, the incipient wax content also increases. Similarly, the incipient wax content increases with an increase in the wall temperature. The mathematical model shows an excellent agreement with experimental data. The aspect ratio of the wax crystals is found to be a strong function of the flow rate of the oil mixture, and it may be a weak function of the wall temperature.

## Notation

$C_{wbo}$ = initial bulk concentration of wax (kg/m$^3$)
$D_{\text{eff}}$ = effective diffusivity of wax inside the gel (m$^2$/s)
$D_{wo}$ = molecular diffusivity of wax in oil (m$^2$/s)
$F_w$ = weight fraction of solid wax in the gel
$Gz_h$ = Graetz number for heat transfer
$Gz_m$ = Graetz number for mass transfer
$h_h$ = heat-transfer coefficient (W/m$^2$/K)
$k_l$ = mass-transfer coefficient (m/s)
$k_e$ = effective thermal conductivity of the gel (W/m/K)
$k_{\text{oil}}$ = thermal conductivity of oil (W/m/K)
$k_{\text{wax}}$ = thermal conductivity of wax (W/m/K)
$L$ = length of the flow loop (m)
$Nu$ = Nusselt number
$Pr$ = Prandtl number
$\bar{r}_i$ = average radius available for oil flow (m)
$R$ = radius of the flow loop (m)
$V_R$ = total volume in the closed system (m$^3$)
$x$ = axial location in the flow loop
$y$ = dimensionless thickness
$\bar{y}$ = average dimensionless thickness
$\Delta H_f$ = heat of solidification of wax (J/kg)
$\mu$ = viscosity of oil (Pa·s)

### *Dimensionless quantities*

$Re$ = Reynolds number, $2Q\rho/\pi r\mu$
$Pr$ = Prandtl number, $\mu C_p/k$
$Sc$ = Schmidt number, $\mu/\rho D$
$Gz_h$ = Graetz number for heat transfer, $(Re \times Pr \times 2R)/x$
$Gz_m$ = Graetz number for mass transfer, $(Re \times Sc \times 2R)/x$

## Literature Cited


Bern, P. A., V. R. Withers, and J. R. Cairns, ''Wax Deposition in Crude Oil Pipelines,'' *Proc. Euro. Offshore Petrol. Conf. and Exhib.*, London, p. 571 (1980).

Bott, T. R., ''Aspects of Crystallization Fouling,'' *Exp. Thermal and Fluid Sci.*, **14**, 356 (1997).

Brown, T. S., V. G. Niesen, and D. D. Erickson, ''Measurement and Prediction of the Kinetics of Paraffin Deposition,'' *Proc. SPE Technical Conf. and Exhib.*, Houston, p. 353 (1993).

Burger, E. D., T. K. Perkins, and J. H. Striegler, ''Studies of Wax Deposition in the Trans Alaska Pipeline,'' *J. Pet. Tech.*, **33**, 1075 (1981).

Carslaw, H. S., and J. C. Jaeger, *Conduction of Heat in Solids*, Oxford Press, Clarendon, 2nd ed. (1959).

Clavell-Grunbaum, D., H. L. Strauss, and R. G. Snyder, ''Structure of Model Waxes: Conformational Disorder and Chain Packing in Crystalline Multicomponent *n*-Alkane Solid Solutions,'' *J. Phys. Chem.*, **101**, 335 (1997).

Cussler, E. L., S. E. Hughes, W. J. Ward, and R. Aris, ''Barrier Membranes,'' *J. Memb. Sci.*, **38**, 161 (1988).

Dirand, M., V. Chevallier, E. Provost, M. Bouroukba, and D. Petitjean, ''Multicomponent Paraffin Waxes and Petroleum Solid Deposits: Structural and Thermodynamic State,'' *Fuel*, **77**, 1253 (1998).

Dorset, D. L., and R. G. Snyder, ''Crystal Structure of Modulated n-Paraffin Binary Solids,'' *J. Phys. Chem.*, **100**, 9848 (1996).

Dorset, D. L. ''Structural Interactions between *n*-Paraffins and Their Perdeuterated Analogues: Binary Compositions with Identical Chain Lengths,'' *Macromol.*, **24**, 6521 (1991).

El-Hattab, M. I., ''Scale Deposition in Surface and Subsurface Production Equipment in the Gulf of Suez,'' *J. Pet. Tech.*, **37**, 1640 (1985).

Hamouda, A. A., and S. Davidsen, ''An Approach for Simulation of Paraffin Deposition in Pipelines as a Function of Flow Characteristics with Reference to a Tesside Oil Pipeline,'' *Proc. SPE Int. Symp. on Oilfield Chemistry*, San Antonio, p. 213 (1995).

Hamouda, A. A., and B. K. Viken, ''Wax Deposition Mechanism Under High Pressure and in Presence of Light Hydrocarbons,'' *Proc. SPE Int. Symp. on Oilfield Chemistry*, New Orleans, p. 385 (1993).

Hausen, H., ''Darstellung des Wärmeuberganges in Rohren durch verallgemeinerte Potenzbeziehungen,'' *VDI Z.*, **4**, 91 (1943).

Hayduk, W., and B. S. Minhas, ''Correlations for Prediction of Molecular Diffusivities in Liquids,'' *Can. J. Chem. Eng.*, **60**, 295 (1982).

Holder, G. A., and J. Winkler, ''Wax Crystallization from Distillate Fuels: I. Cloud and Pour Phenomena Exhibited by Solutions of Binary n-Paraffin Mixtures,'' *J. Inst. Petrol.*, **51**, 228 (1965a).

Holder, G. A., and J. Winkler, ''Wax Crystallization from Distillate Fuels, Part II. Mechanism of Pour Depression,'' *J. of Inst. Petrol.*, **51**, 235 (1965b).

Lee, K. S., W. S. Kim, and T. H. Lee, ''A One-Dimensional Model for Frost Formation on a Cold Flat Surface,'' *J. Heat Mass Transfer*, **40**, 4359 (1997).

Létoffé, J. M., P. Claudy, M. V. Kok, M. Garcin, and J. L. Volle,

''Crude Oils: Characterization of Waxes Precipitated on Cooling by D.S.C. and Thermomicroscopy,'' *Fuel*, **74**, 810 (1995).
Majeed, A., B. Bringedal, and S. Overa, ''Model Calculates Wax Deposition for N. Sea Oils,'' *Oil Gas J.*, **88**, 63 (1990).
Neto, F. R. A., J. N. Cardoso, and A. S. Pereira, ''Application of High Temperature High Resolution Gas Chromatography to Paraffinic Deposits in Petroleum Production Pipelines,'' *J. High Res. Chrom.*, **17**, 259 (1994).
Pierre, A. C., K. Ma, and C. Barker, ''Structure of Kaolinite Flocs Formed in an Aqueous Medium,'' *J. Mat. Sci.*, **30**, 2176 (1995).
Ribeiro, F. S., P. R. S. Mendes, and S. L. Braga, ''Obstruction of Pipelines due to Paraffin Deposition During the Flow of the Crude Oil,'' *Int. J. Heat Mass Transfer*, **40**, 4319 (1997).
Seider, E. N., and C. E. Tate, ''Heat Transfer and Pressure Drop of Liquids in Tubes,'' *Ind. Eng. Chem.*, **28**, 1429 (1936).
Singh, P., and H. S. Fogler, ''Fused Chemical Reactions: The Use of Dispersion to Delay Reaction Time in Tubular Reactors,'' *Ind. Eng. Chem. Res.*, **37**, 2203 (1998).
Singh, P., H. S. Fogler, and N. Nagarajan, ''Prediction of the Wax Content of the Incipient Wax-Oil Gel in a Flowloop: An Application of the Controlled-Stress Rheometer,'' *J. Rheol.*, **43**, 1437 (1999).
Srivastava, S. P., J. Handoo, K. M. Agrawal, and G. C. Joshi, ''Phase-Transition Studies in *n*-Alkanes and Petroleum Related Waxes: A Review,'' *J. Phys. Chem. Solids*, **54**, 639 (1993).
Svendsen, J. A., ''Mathematical Modeling of Wax Deposition in Oil Pipeline Systems,'' *AIChE J.*, **39**, 1377 (1993).
Tao, Y. X., R. W. Besant, and K. S. Rezkallah, ''A Mathematical Model for Predicting the Densification and Growth of Frost on a Flat Plate,'' *Int. J. Heat Mass Transfer*, **36**, 353 (1993).
Wardhaugh, L. T., and D. V. Boger, ''The Measurement and Description of the Yielding Behavior of Waxy Crude Oil,'' *J. Rheol.*, **35**, 1121 (1991).

## Appendix: Calculation of the Molecular Diffusivity of Wax in Oil

Hayduk and Minhas (1982) proposed a correlation to predict the molecular diffusivity $D_{wo}$ of paraffins in paraffinic solvents with an average error of 3.4% which is

$$D_{wo} = 13.3 \times 10^{-8} \times \frac{T^{1.47} \mu^{\gamma}}{V_A^{0.71}} \text{ cm}^2/\text{s}, \qquad \text{(A1)}$$

where $T$ is absolute temperature (K), $\mu$ is solvent viscosity (mPa·s), $V_A$ is molar volume of the paraffin (cm$^3$/mol), and $\gamma$ is a function of $V_A$ defined as

$$\gamma = \frac{10.2}{V_A} - 0.791.$$

For a typical wax-oil sample, the average molecular weight of paraffin molecules is 400. The density of the wax 0.9 g/cm$^3$. The molar volume is

$$V_A = 435 \text{ cm}^3/\text{mol}, \quad T = 287.5 \text{ K}, \quad \mu = 8.0 \text{ mPa} \cdot \text{s}$$

The correlated value of the diffusivity is $D_{wo} = 1.48 \times 10^{-06}$ cm$^2$/s.

*Manuscript received Aug. 19, 1999, and revision received Dec. 28, 1999.*